Journal of
Composites Science

MDPI

Article

Enhancing the Fracture Toughness Properties by Introducing Anchored Nano-Architectures at the Metal–FRP Composite Interface

Ghowsalya Mahendrarajah, Everson Kandare and Akbar A. Khatibi *

Sir Lawrence Wackett Aerospace Research Centre, School of Engineering, RMIT University, Melbourne, VIC 3001, Australia; ghowsalya.mahendrarajah@student.rmit.edu.au (G.M.); everson.kandare@rmit.edu.au (E.K.)

* Correspondence: akbar.khatibi@rmit.edu.au; Tel.: +61-3-9925-6105

Received: 30 December 2018; Accepted: 11 February 2019; Published: 13 February 2019

Abstract: This paper presents a novel technique for improving aluminium–glass/epoxy composite interfacial bonding through the generation of metallic nano-architectures on the metal surface. Silver nanowires (AgNWs) deposited via solution casting at varying concentrations and annealed at different temperatures in an air atmosphere improved the aluminium-glass/epoxy composite fracture toughness as measured via mode I experiments. For AgNW concentrations of 1 and 3 g/m^2 deposited via a single-stage process and annealed at 375 °C, the initiation fracture toughness of the aluminium-glass/epoxy composite improved by 86% and 157%, respectively, relative to the baseline composite without AgNWs. The corresponding steady-state fracture toughness of these nano-modified fibre metal laminates (FMLs) were at least seven times greater than the baseline composite. The FML variant in which AgNWs were deposited at a concentration of 3 g/m^2 through a two-stage process followed by annealing at 375 °C and 300 °C, respectively after each deposition, achieved the highest steady-state fracture toughness of all nano-modified composites—a fracture toughness value that was 13 times greater than the baseline composite. Intrinsic and extrinsic toughening mechanisms dictated by the morphology of the silver nano-architectures were found to be responsible for the improved initiation and steady-state fracture toughness in nano-modified FMLs.

Keywords: fibre metal laminates (FMLs); interleaving; mode I fracture toughness

1. Introduction

Aluminium alloys and fibre-reinforced polymer (FRP) composites account for the greatest proportion of materials used in the aerospace industry. Although they offer high-impact resistance, aluminium alloys are susceptible to stress-corrosion cracking which can lead to unexpected sudden failure of components subjected to tensile loading [1]. On the other hand, FRP composites exhibit excellent fatigue properties, high resistance to corrosion and more importantly, exceptional structural efficiency [2]. However, FRP composites suffer from low fracture toughness at the ply–ply interface making them vulnerable to impact-induced through thickness damage. Hybridised material systems constituting of alternating layers of metal and FRP laminates, generally referred as fibre metal laminates (FMLs), offer alternative structural materials possessing unique and desirable properties of both the metal and the FRP composite [3–6]. The certification of the glass reinforced aluminium laminate, commercially identified as GLARE® for use in the Airbus380 upper fuselage demonstrates technological maturity and economic viability of FML composites in aerospace engineering. Nonetheless, despite their desirable characteristics, the durability and continuing airworthiness of FML composite structures is strongly linked to the interfacial strength between the

metal sheets and FRP laminates [4,5,7]. Because of the dissimilar constituent material properties, FMLs are prone to delamination cracking along the metal–FRP composite interface. Interfacial defects manifesting from manufacturing errors, stress concentrations in the vicinity of cut-outs and low-velocity impact (e.g., tool drops) can grow into delamination cracks that may threaten the structural integrity of the FML composite [8]. It is therefore critical to develop technologies that can improve the interfacial adhesion between the metal and FRP composite layer.

To this end, several techniques including mechanical (i.e., surface machining, abrasion), chemical (i.e., coupling agents, matrix modification) and electrochemical (i.e., electrolytic etching) and dry surface treatments such as plasma treatments [9–12], ion-beam enhanced deposition (IBED) [5,13] and laser texturing [11,14,15], have been used to improve the metal–FRP composite interfacial strength [13,16–23]. Ning et al. [23] demonstrated that mechanical abrasion (i.e., sanding or grit-blasting) coupled with acid etching of the aluminium adherend can significantly improve the mode I fracture toughness of FMLs. Other researchers have incorporated multi-scale toughening agents (i.e., carbon-based nanomaterials) into the polymeric adhesive interfacial layer between the metal substrate and the FRP composite yielding significantly improved fracture toughness [24–27]. The integration of multi-scale matrix-toughening agents at the metal–FRP composite interface can be extended to the insertion of an additional reinforcing phase (i.e., an interleaf) between the metal and FRP composite adherends. Sun et al. [26,27] incorporated short aramid fibres in the form of a non-woven mat to improve the fracture toughness of the epoxy adhesive between the aluminium substrate and a carbon fibre polymer composite. The interfacial fracture toughness of the aramid fibre-enhanced adhesive joints was found to be significantly greater than the corresponding value measured for the baseline composite. In a comparable research study, Ning et al. [28] integrated nano-fillers in the form of a vapour-grown carbon fibre (VGCF) interleaf with the filler concentration of 10 g/m^2 at the aluminium–carbon fibre composite to achieve more than 40 times enhancement in the initiation fracture toughness properties relative to the baseline composite without an interleaf. The same authors extended their research to investigate the effectiveness of the VGCF interleaf on the mode II fracture toughness of glass fibre-reinforced plastic (GFRP)/aluminium [19] and carbon fibre-reinforced polymer (CFRP)/aluminium [22] composites. The presence of the carbon nano-fibre interleaf respectively increased the mode II fracture toughness at the GFRP/aluminium and CFRP/aluminium interface by 175% and 385% relative to the composites without any reinforcements.

While the insertion of an interleaf at the metal–FRP composite interface has been demonstrated to improve the fracture toughness properties, this technique may not be reaching its full potential due to the absence of physical bonding to either the metal or FRP composite adherend. Recently, Nguyen et al. [29] used the selective laser melting (SLM) to manufacture titanium metal sheets incorporating micro- and macro-features (e.g., grooves or dimples) to improve the bonding of titanium to carbon epoxy composite laminates. These authors established that micro-scale (10–15 μm) surface roughness achieved relatively high fracture toughness of 1.20 kJ/m^2. In a separate but related study by the same research group, the Double Cantilever Beam (DCB) tests showed that the integration of SLM-printed pins (nominally 0.5% of specimen volume) increased the maximum load, initiation fracture toughness and steady-state fracture toughness by 270%, 250% and 377% respectively, provided pins were designed to pull out of the composite and not fracture [30]. However, in both studies, the metal adherends having distinct surface morphologies were manufactured as single piece using the additive metal printing technology. So far, there has not been any attempt to introduce similar surface features onto pre-fabricated metal substrates. It is, therefore, unknown whether similar fracture toughness improvements to those observed by Nguyen et al. [29,30] can be achieved by 3D-printing surface features onto pre-fabricated metal substrates.

In the present study, we therefore set out to investigate the feasibility of creating interleaf-like multi-scale surface architectures physically bonded (i.e., chemical or metallic) to the metal adherend. In addition to the intrinsic toughening due to the presence of an interleaf at the metal–FRP composite interface, we envisaged that the extra energy required to dislodge the anchored (i.e., physically bonded) interleaf from the metal adherend during crack propagation would further enhance the

fracture toughness properties. To that effect, we exploited the well-established knowledge that metallic nanowires can fuse with each other or with bulk metallic substrates at relatively low temperatures in the absence of applied pressure [31–41]. Physically bonding (i.e., anchoring) toughening nano-architectures onto the metal adherend has the potential to reduce the filler concentration without compromising the fracture toughness, thereby effectively increasing the structural efficiency of FML composites. Prior to the deposition of silver nanowires (AgNWs), the aluminium adherend was mechanically abraded and acid-etched to promote physical bonding with the nanowires. Leaving the annealing conditions unchanged, the effect of AgNW concentration on the mode I fracture toughness of the GFRP/aluminium FML composite was investigated. Coupled with the exploration of the effect of annealing conditions on the morphology of silver nano-architectures generated on the aluminium adherend surface, we investigated the correlation between the ensuing surface morphology to the mode I fracture toughness properties. Using fractographic analysis of the fractured delamination surfaces, toughening mechanisms and their dependency on the nano-texture morphology of the aluminium adherends were investigated.

2. Materials and Methods

Aluminium 2024-T3, an aerospace grade alloy, was obtained from Airport Metals, Australia. Plain woven glass fabric AF251140 (E-Glass; 185 gsm) obtained from Colan Australia was impregnated with West system epoxy resin (105 resin and 206 slow hardener) and used to manufacture FRP laminates. Silver nanowires (AgNWs) were supplied by ACS Materials, USA in the form of an ethanol suspension of AgNWs (diameter = 120 nm; length = 20 microns) with a nominal concentration of 25 mg/mL.

The aluminium alloy strips (200 mm × 25 mm × 1.5 mm) were mechanically abraded using a pneumatic orbital sander operated with a P40/240-grit sandpaper to remove the protective surface aluminium oxide layer. The sanded aluminium strips were then acid-etched by immersing in a 2M solution of nitric acid (HNO_3) in distilled water for 24 h. Following the acid etching process, the aluminium strips were rinsed with distilled water and left to dry at ambient conditions. The AgNW suspension was ultrasonically-treated using the Hielscher UP200PS ultrasonic processor (power = 85%, pulse rate = 0.5 s, temperature = 23 °C, time = 2 min) to achieve a homogenous distribution of the nanowires in ethanol. The AgNW/ethanol suspension was deposited in desired quantities on the surface-treated aluminium substrates via drop-casting using a syringe.

In the present work, two concentrations of 1 and 3 g/m^2 were deposited via either a single- or two-stage deposition process. For the single-stage deposition, the desired amount of AgNWs was deposited uniformly onto the acid-etched aluminium surface with the solvent (ethanol) left to evaporate under ambient conditions (23 °C; 1 atm). The aluminium strip was then heat-treated at 375 °C in a furnace for 1 h. For the two-stage deposition, half the target AgNW concentration was deposited followed by solvent drying and heat treatment at 375 °C in a furnace for 1 h. The aluminium strip was then removed from the furnace and allowed to naturally cool down to room temperature before the second half of the desired concentration of AgNWs was deposited. Following the second deposition, the aluminium strip was heat-treated at 300 °C in a furnace for another hour. A relatively lower temperature, 300 °C, for the second stage was sufficient to achieve nano-bonding between the AgNWs without causing significant changes to their aspect ratio. The single-stage deposition process was conceptualised to produce globular silver features on the aluminium surface while the two-stage deposition process was designed to create web-like nano-features along with globular features on the aluminium surface as illustrated in Figure 1.

The resin and slow hardener of West System epoxy resin system (105 and 206, respectively) were mixed in the ratio of 5:1 and 16 layers of plain-woven [0/90] glass fabric were impregnated by wet layup process at a fibre-to-resin ratio of 1:1 and stacked together to achieve the laminate configuration $[0/90]_{16}$. The resulting laminate had an average thickness of 2.25 mm and fibre volume fraction (FVF) of 32%. The required thickness of the FRP layer was calculated using Classical Beam Theory to match the bending stiffness of the aluminium strip and the composite layer. The aluminium strips

(with/without nano-features) were placed onto a single large composite laminate with the treated surface at the metal–laminate interface. A thin aluminium foil (thickness—16µm), coated with Zyvax® EnviroShield™ release agent, was placed at one end of the aluminium–laminate interface to serve as the crack initiator. The aluminium/composite laminate layup was vacuum-bagged and cured at room temperature for 24 h. The cured aluminium/laminate composite was cut into individual DCB test specimens (200 mm × 25 mm) and subjected to mode I fracture toughness test after 96 h as per the recommendation of the manufacturer (this is the time after which the resin attains its maximum strength). The FML variants tested were identified as *x*g-*n*s where '*x*' denotes the concentration of AgNWs (1 or 3 g/m^2) while '*n*' denotes the deposition process (single (1)- or two (2)-stage). The FML configuration investigated in this study are given in Table 1.

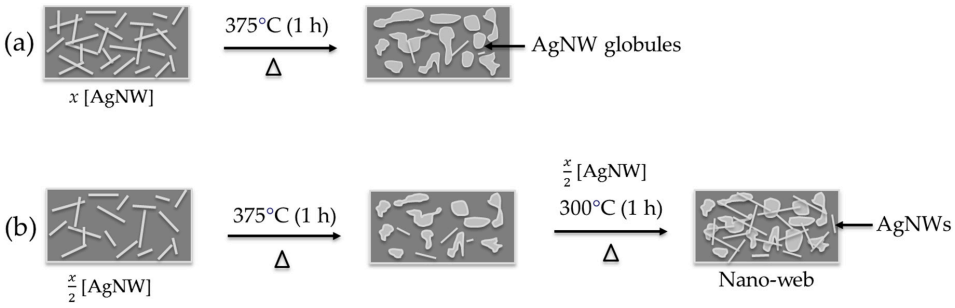

Figure 1. (**a**) Single-stage and (**b**) two-stage silver nanowire deposition. [AgNW] represents the concentration of nanowires deposited at each stage.

Table 1. Fibre Metal Laminate (FML) variants investigated for mode I fracture toughness properties.

FML Configuration	AgNW Concentration (g/m^2)	No. of Deposition Stages
0g-0s *	0.0	0
1g-1s	1.0	1
3g-1s	3.0	1
3g-2s	3.0	2

* The specimen 0g-0s represent the baseline composite without AgNWs.

The mode I fracture toughness properties of the FML composites were evaluated using the DCB specimens in accordance with the ASTM Standard D5528. To preclude the breakage of test specimens during loading due to potentially enhanced fracture toughness, 16-ply unidirectional carbon fibre-epoxy (VTM264) composite laminates were bonded onto the DCB specimens using Araldite 420, an epoxy-based adhesive supplied by Huntsman®. A schematic of the DCB specimen showing the geometry and dimensions is shown in Figure 2.

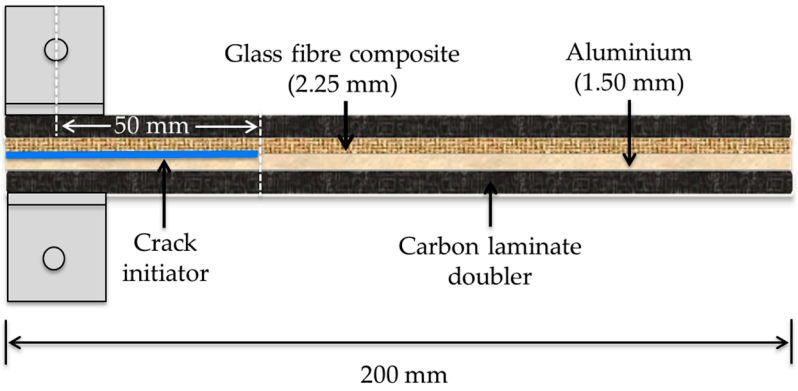

Figure 2. Geometry and dimensions of the Double Cantilever Beam (DCB) specimens used for measuring the fracture toughness properties.

Fracture toughness measurements were conducted under displacement control using an Instron machine with a load capacity of 10 kN. The crack opening displacement (COD) was increased at a rate of 1 mm/min with the crack growth at the aluminium–laminate interface measured using an optical microscope. The mode I fracture toughness, G_{Ic}, was then calculated via the modified beam theory in accordance to the ASTM Standard D5528 using the expression:

$$G_{Ic} = \frac{3}{2}\frac{P\delta}{b(a+|\Delta|)} \quad (1)$$

where P = is the applied COD load, δ = is the crack opening displacement, b is the specimen width, a is the total crack length while Δ is the experimentally determined correction factor to account for rotation at the crack front. Five specimens were evaluated for each FML configuration. High resolution images of the nano-modified aluminium and the DCB fracture surfaces were collected using the FEI Nova NanoSEM or Verios 460L scanning electron microscopes (SEM).

3. Results

Figure 3 shows the SEM images of aluminium surfaces nano-modified at different temperatures following either the single- or two-stage deposition process. The single-stage deposition followed by heat-treatment at 300 °C resulted in a forest of interconnected AgNWs which largely retained their aspect ratios (Figure 3a). Increasing the processing temperature from 300 to 375 °C caused the AgNWs to melt and form surface-bonded *globules* as evident from Figure 3b. The two-stage deposition process, involving an initial heat-treatment at 375 °C followed by the deposition of the remaining half of the AgNWs and a secondary heat-treatment at 300 °C, resulted in an intertwined nano-web of micro-sized silver globules and nanowires (Figure 3c). It is noteworthy that the dissimilarities in the aluminium surface features due to varied deposition processes should allow for tuneable fracture toughness properties at the metal–FRP composite interface.

As revealed by the close-up SEM images of the nano-modified aluminium surfaces in Figure 4, metallic bonding was created between AgNWs and aluminium substrate as a result of the nano-bonding procedure. Figure 4c shows AgNWs anchored within micro-sized crevices on the aluminium surface. In instances where the AgNWs were oriented normal to the aluminium sheet, they were expected to contribute to improved metal–FRP laminate fracture toughness as demonstrated by Nguyen and others [23,24] for hybrid metal-composite joints with integrated 3D-printed metallic reinforcements. Figure 4a provides evidence for metallic bonding of AgNWs along their axial lengths to the aluminium substrate. The AgNWs oriented along the aluminium surface may contribute towards improved fracture toughness via strain energy dissipated as they peel-off the metal surface during the crack propagation phase. Pressure-less metal-metal bonding of the AgNWs is evident from the SEM image shown in Figure 4b. The presence of a silver nano-web at the metal–FRP laminate interface has the potential to slow down delamination crack growth via a suite of toughening mechanisms that may include crack arrest, crack deflection, matrix crack-bridging, plastic deformation and fracture of the nano-web as well as surface peel-off.

The effect of aluminium surface modification (i.e., AgNW concentration and/or deposition process) on the mode I crack growth resistance (R) curve at the metal–laminate interface is shown in Figure 5. The baseline FML composite (without AgNWs) yielded an R-curve exhibiting relatively low and unchanging fracture toughness with increasing crack length. In contrast, the R-curves for nano-reinforced FMLs revealed gradual increases in the fracture toughness within the initial crack growth phases (0–40 mm crack length) and reached steady-state fracture toughness values at crack length values above 40 mm.

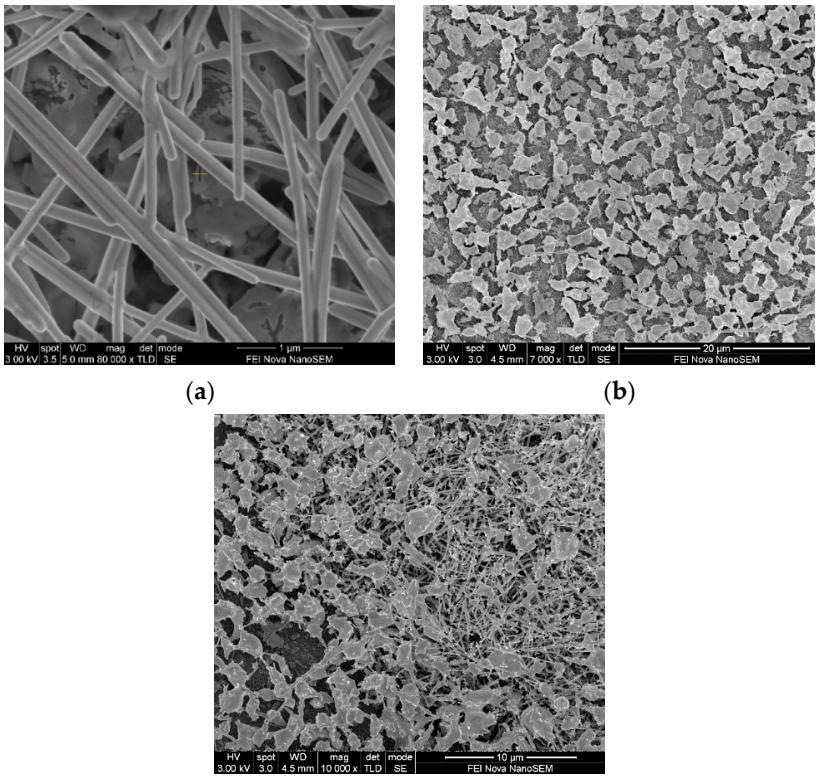

Figure 3. SEM images of AgNW-modified aluminium surfaces (**a**) single-stage deposition at 300 °C, (**b**) single-stage deposition at 375 °C and (**c**) two-stage deposition (375 °C followed by 300 °C).

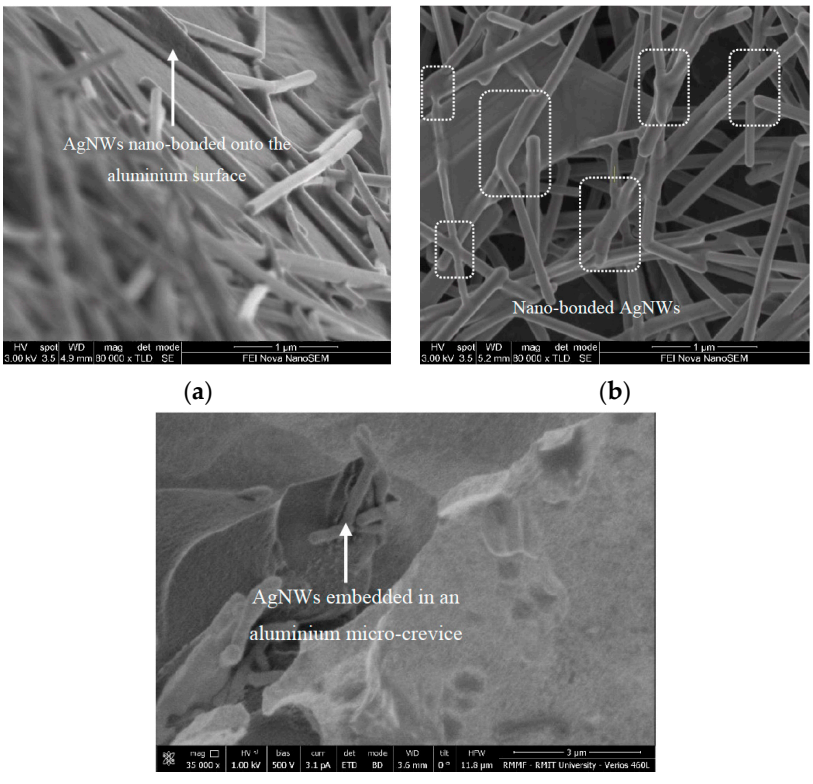

Figure 4. SEM images of AgNW-modified aluminium surfaces showing nanowires (**a**) bonded (metallic) to aluminium and (**b**) to each other and (**c**) embedded in aluminium micro-crevices.

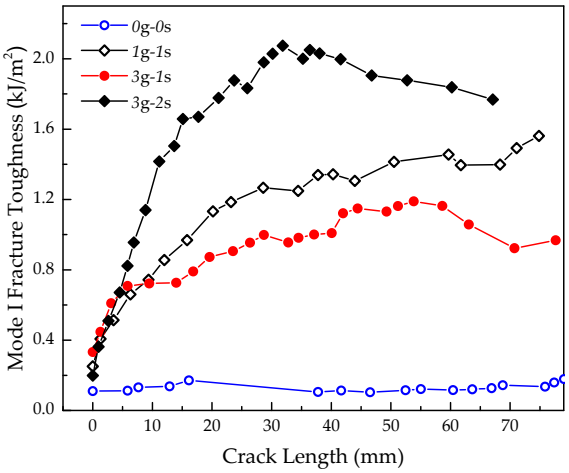

Figure 5. Representative growth resistance (R)-curves for FMLs obtained from mode I experiments.

The critical initiation toughness ($G_{Ic,i}$) and the steady-state (crack propagation) toughness ($G_{Ic,ss}$) determined via mode I experiments for the baseline and AgNW-modified composites is given in Table 2. It should be noted that in this study, $G_{Ic,ss}$ was calculated by averaging the measured fracture toughness values between the crack length values of 40 and 80 mm. For the single-stage deposition, the strain energy release rate for crack initiation increased with increasing AgNW concentration. Compared to the baseline composite, the FML composites incorporating 1 and 3 g/m^2 of AgNWs revealed 86% (from 0.14 to 0.26 kJ/m^2) and 157% (from 0.14 to 0.36 kJ/m^2) improvements in the initiation toughness. The change in the deposition process from single to two stages did not alter the initiation fracture toughness with the measured $G_{Ic,i}$ value for 3g-2s (0.28 $\pm$ 0.12 kJ/m^2) comparable to that of the 3g-1s composite (0.36 $\pm$ 0.14 kJ/m^2).

Table 2. Initiation and steady-state fracture toughness values determined via mode I experiments.

FML Configuration	Initiation Fracture Toughness (kJ/m^2)	Steady-State Fracture Toughness (kJ/m^2)
0g-0s *	0.14 $\pm$ 0.06	0.14 $\pm$ 0.05
1g-1s	0.26 $\pm$ 0.06	1.31 $\pm$ 0.25
3g-1s	0.36 $\pm$ 0.14	1.06 $\pm$ 0.19
3g-2s	0.28 $\pm$ 0.12	2.09 $\pm$ 0.28

* The specimen 0g-0s represent the baseline composite without AgNWs.

The steady-state fracture toughness increased by ~900% for the 1g-1s FML variant relative to the baseline composite. Keeping the deposition process invariable, the increase in the AgNW concentration from 1 to 3 g/m^2 did not yield further enhancements in the steady-state fracture toughness. The SEM images of nano-modified aluminium specimen containing 3 g/m^2 of the AgNWs revealed relatively larger number of silver *globules* than those observed for the 1g-1s FML composite. The aluminium surface roughness is, therefore, likely to decrease with the increasing surface coverage by the silver *globules* leading to a reduction in crack propagation resistance at the metal–FRP laminate interface. This observation suggests that there is an optimum *globule* size and area density beyond which the steady-state toughening effect of such surface features (silver *globules*) begin to diminish. This proposition is further supported by the distinct steady-state fracture toughness measured for the FML composite containing the same amount of AgNWs (3 g/m^2) but modified via a two-staged deposition process. Despite having similar R-curve growth rates within the initial 20 mm of delamination crack length, the steady-state fracture toughness measured for 3g-2s is nearly twice as high (2.09 $\pm$ 0.28 kJ/m^2) as that measured for the 3g-1s FML (1.06 $\pm$ 0.19 kJ/m^2). The high fracture toughness of 3g-2s specimens can be attributed to complex fracture behaviour where the crack has propagated inside of the composite layer, as evident from Figure 6.

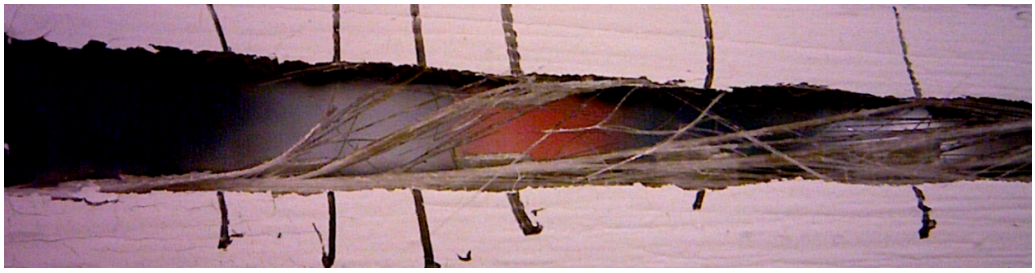

Figure 6. Crack propagation into the composite layer in a 3g-2s specimen.

4. Discussion

Fractographic analysis of fractured nano-modified FMLs revealed distinct microscopic features and surface morphologies consistent with well-established toughening mechanisms such as fibre debonding and pull-out, plastic deformation of the matrix around the reinforcing fibres, plastic deformation of the metallic fibres, fibre fracture, metallic fibre peel-off and matrix crack-bridging by the metallic nano-reinforcements. The measured initiation fracture toughness values for nano-modified FMLs were higher than that of the baseline composite. The presence of AgNWs at the interfacial region between the metal and FRP laminate improved the intrinsic toughness of the epoxy matrix leading to relatively higher initiation values.

The triaxial stresses operating ahead of the crack tip caused interfacial debonding due to the mismatch in the epoxy matrix and AgNW stiffness as evident in Figure 7a. It is inevitable that some of the AgNWs aligned along or at an angle to the Z-direction extended into the delamination crack path at the metal-glass/epoxy laminate interface. Thus, behind the crack tip, the debonded AgNWs bridged the crack faces and gradually pulled-out of the matrix as the COD increased (Figure 7a). The traction loads generated by the AgNWs as they pull-out of the matrix reduced triaxial stresses exerted at or ahead of the crack tip thereby effectively increasing the steady-state fracture toughness.

As shown in Figure 3c, the two-stage deposition methodology yielded a web-like 3D interconnected network of aluminium-bonded AgNWs. During the manufacturing of the FML, the liquid epoxy resin inevitably infused and cured around these webbed nano-architectures resulting in the formation of strong mechanical interlocks. Consequently, the energy required to pull-out the intertwined nanowire architectures from the cured epoxy matrix is no doubt greater than in the case where the nanowires exist independently as single unconnected nano-fibres. Furthermore, the interwoven nanowire architectures formed via the two-stage deposition process were likely to exhibit significantly higher bending rigidity than the surrounding matrix. The high-stiffness bundled nanowires pulling-out of the matrix at an angle permanently deformed the surrounding epoxy matrix as shown in Figure 7b. The ensuing matrix void growth relieved the stresses acting at or ahead of the crack tip thereby increasing the resistance to crack propagation. Thus, the presence of interwoven and nano-bonded AgNWs are potentially the primary reason for the increased fracture toughness for the 3g-2s composite relative to its 3g-1s counterpart.

Matrix crack-bridging is another toughening mechanism identified in nano-modified FMLs, as shown in Figure 7c. Due to the triaxial stresses exerted in the vicinity of the crack tip, micro-cracking is typically observed within the process zone. In Figure 7c, there is evidence of AgNWs bridging the matrix micro-cracks thereby potentially arresting and/or deflecting the cracks. Further, the plastic deformation of the matrix crack-bridging AgNWs provided an additional pathway for strain energy dissipation that would have led to improved steady-state fracture properties for nano-modified FMLs. Figure 7d shows surface imprints left behind by AgNWs that peeled off the aluminium adherend during delamination crack growth. The peeled off AgNWs plastically deformed into vertically oriented metal pins, as revealed in Figure 7e. Both the nanowire peel-off and ensuing plastic deformation served to release stored strain energies thus effectively improving the steady-state fracture toughness. Figure 7f reveals fractured AgNWs anchored within the epoxy matrix and exhibiting signs of 'necking'.

The localised plastic deformation (e.g., necking) and the subsequent fracture of the AgNWs are additional extrinsic toughening mechanisms that may have been responsible for the improved fracture toughness properties in nano-modified FMLs.

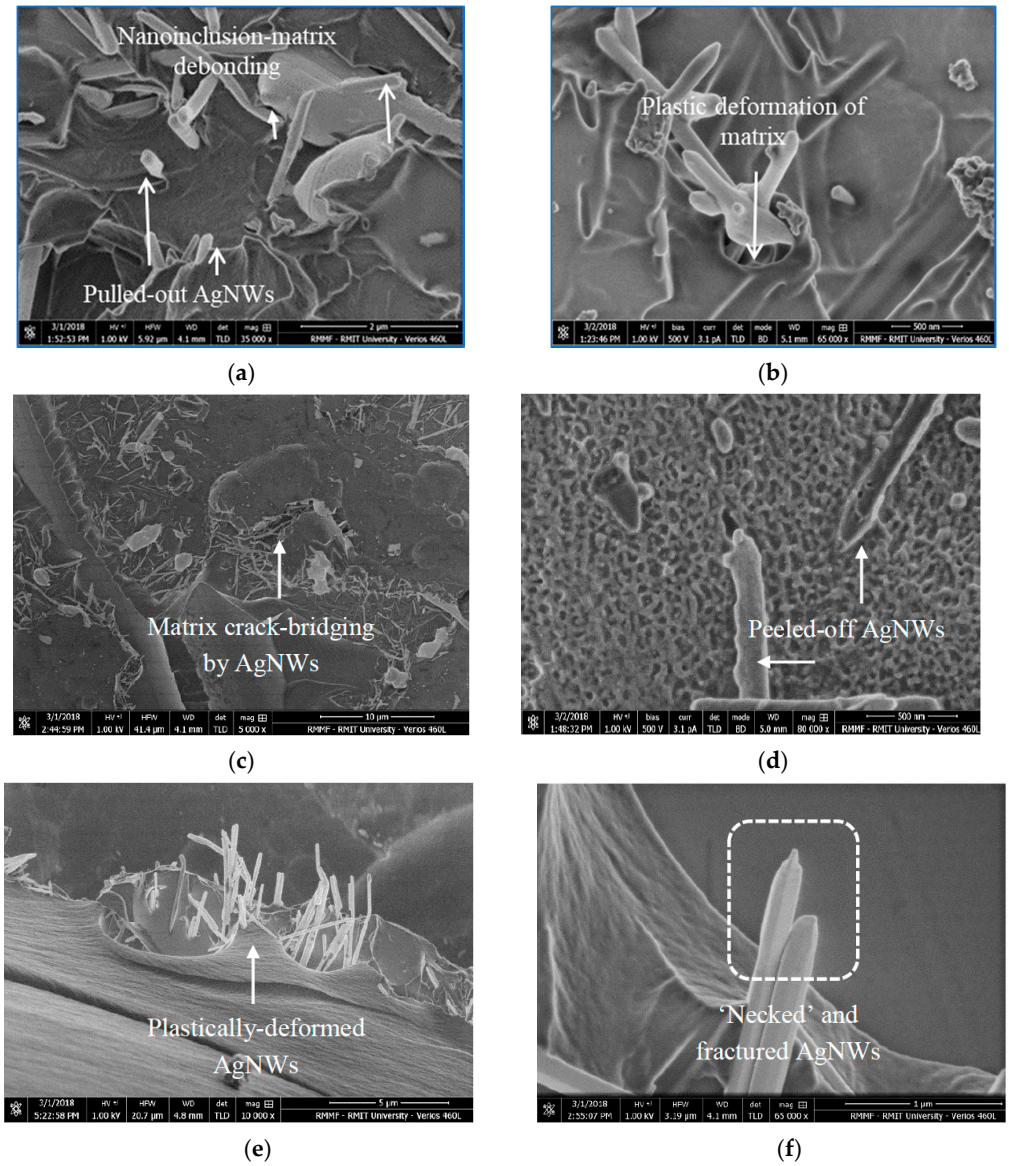

Figure 7. SEM images showing (**a**) debonded and pulled-out AgNWs, (**b**) plastically deformed epoxy matrix, (**c**) matrix crack-bridging by AgNWs, (**d**) aluminium-surface imprints left behind after AgNWs peeled off, (**e**) plastically deformed (i.e., straightened) AgNWs and (**f**) fractured AgNWs revealing localized plastic deformation (i.e., 'necking').

Fractographic analysis of the delamination surfaces of the baseline composite (without AgNWs) revealed relatively smooth fracture surfaces compared to the modified FMLs containing AgNWs. This observation suggests that delamination failure occurred predominantly at the aluminium–FRP composite interface and the smoothness is due to the absence of reinforcements (AgNWs) which increases the fracture toughness via various mechanisms. In nano-modified FMLs, the presence of AgNWs anchored onto the aluminium surface caused the delamination crack to move into the resin-rich and nanowire-reinforced aluminium–FRP composite interface. The matrix toughening effect, brought about by the presence of AgNW architectures, was so effective that it caused the delamination

crack to cross over from the interfacial region into the glass/epoxy laminate as shown in Figure 8 for the 3g-2s composite.

Figure 8. SEM image showing the glass fibres that remained bonded to the aluminium adherend following delamination fracture.

The fractured aluminium surface was covered by glass fibres suggesting that the delamination crack moved into the FRP composite. The meandering of the delamination crack between the FRP composite and the AgNW-enhanced interface increased the fracture surface area, thereby increasing the fracture energy. Furthermore, fibre-bridging of the delamination crack surfaces by the glass fibres may have been partly responsible for the elevated steady-state fracture toughness of the 3g-2s composite.

5. Conclusions

The fracture toughness of the aluminium–glass/epoxy composite laminate interface was improved by creating nano-structured architectures on the aluminium surface. The deposition of varied concentrations of AgNWs onto the aluminium substrate followed by annealing at different temperatures enabled the creation of anchored silver nano-architectures with tuneable morphologies. The fracture toughness at the aluminium-glass/epoxy composite interface was tailored by varying either the metal nanowire concentration or the annealing conditions. Evaluation of mode I fracture toughness of the nano-modified FMLs revealed that:

- For the single-stage deposition, the initiation fracture toughness increased with the incorporation of AgNWs regardless of the concentration, at least for the range considered in this study.
- The steady-state fracture toughness for the single-stage deposition FML was insensitive to changes in the AgNW concentration under invariable annealing conditions. Similar steady-state fracture toughness values were measured for 1g-1s and 3g-1s.
- The steady-state fracture toughness was found to be dependent on the morphology (e.g., form, size, shape and structure) of the AgNW architectures which was dictated by the deposition technique. The $G_{Ic,ss}$ value measured for 3g-2s (2.09 ± 0.28 kJ/m^2) is significantly higher than that of the 3g-1s composite (1.06 ± 0.19 kJ/m^2) despite the invariable AgNW concentration.
- Fracture initiation toughness was found to be controlled by the presence of the nano-reinforcements within the polymer matrix while the steady-state fracture toughness was determined by the silver nano-architecture morphology.
- The enhanced fracture toughness properties of the nano-modified FMLs resulted from both intrinsic and extrinsic toughening mechanisms triggered by the presence of AgNW architectures within the metal–FRP laminate interfacial region. Some of the toughening mechanisms identified through SEM analysis of the delamination surfaces included nanowire-epoxy matrix debonding, nanowire pull-out and peel-off from the aluminium surface, plastic deformation and subsequent fracture of the AgNWs, plastic deformation of the matrix due to the subbing caused by bundled nanowires, as well as the matrix crack-bridging by AgNWs.

Overall, this study revealed that the incorporation of AgNWs at the aluminium–glass/epoxy composite interface coupled with controlled deposition-annealing processes led to tailored improvements in the initiation and steady-state fracture toughness of the modified FMLs.

Author Contributions: Conceptualization, G.M.; Methodology, G.M., E.K. and A.K.; Formal Analysis, G.M.; Investigation, G.M.; Resources, E.K. and A.K.; Data Curation, G.M.; Writing–Original Draft Preparation, G.M.; Writing–Review & Editing, G.M., E.K. and A.K.; Visualization, G.M., E.K. and A.K.; Supervision, E.K. and A.K.; Project Administration, A.K.; Funding Acquisition, A.K.

Funding: One of the authors (G.M.) acknowledges the research support through the Australian Postgraduate Award (APA).

Acknowledgments: The authors acknowledge the technical support by Peter Tkatchyk and Julian Bradler and the SEM technical guidance provided by the team at RMIT's RMMF facility.

Conflicts of Interest: The authors declare no conflict of interest.

References

1. Starke, E.A., Jr.; Staley, J. Application of modern aluminum alloys to aircraft. *Prog. Aerosp. Sci.* **1996**, *32*, 131–172. [CrossRef]
2. Zhang, X.; Chen, Y.; Hu, J. Recent advances in the development of aerospace materials. *Prog. Aerosp. Sci.* **2018**, *97*, 22–34. [CrossRef]
3. Vogelesang, L.B.; Vlot, A. Development of fibre metal laminates for advanced aerospace structures. *J. Mater. Process. Technol.* **2000**, *103*, 1–5. [CrossRef]
4. Wu, G.; Yang, J.-M. The mechanical behavior of GLARE laminates for aircraft structures. *JOM* **2005**, *57*, 72–79. [CrossRef]
5. Sinmazcelik, T.; Avcu, E.; Bora, M.Ö.; Çoban, O. A review: Fibre metal laminates, background, bonding types and applied test methods. *Mater. Des.* **2011**, *32*, 3671–3685. [CrossRef]
6. Asundi, A.; Choi, A.Y. Fiber metal laminates: An advanced material for future aircraft. *J. Mater. Process. Technol.* **1997**, *63*, 384–394. [CrossRef]
7. Ostapiuk, M.; Surowska, B.; Bieniaś, J. Interface analysis of fiber metal laminates. *Compos. Interfaces* **2014**, *21*, 309–318. [CrossRef]
8. Remmers, J.; De Borst, R. Delamination buckling of fibre–metal laminates. *Compos. Sci. Technol.* **2001**, *61*, 2207–2213. [CrossRef]
9. Carrino, L.; Napolitano, G.; Sorrentino, L. Wettability improving of 2024 aluminium alloy by oxygen cold plasma treatment. *Int. J. Adv. Manuf. Technol.* **2006**, *31*, 465–473. [CrossRef]
10. Davis, G.D.; Groff, G.B.; Zatorski, R.A. Plasma Spray Coatings as Treatments for Aluminum, Titanium and Steel Adherends. *Surf. Interface Anal.* **1997**, *25*, 366–373. [CrossRef]
11. Fernandes, J.C.S.; Ferreira, M.G.S.; Haddow, D.B.; Goruppa, A.; Short, R.; Dixon, D.G. Plasma-polymerised coatings used as pre-treatment for aluminium alloys. *Surf. Coat. Technol.* **2002**, *154*, 8–13. [CrossRef]
12. De Iorio, I.; Leone, C.; Nele, L.; Tagliaferri, V. Plasma treatments of polymeric materials and Al alloy for adhesive bonding. *J. Mater. Process. Technol.* **1997**, *68*, 179–183. [CrossRef]
13. Park, S.Y.; Choi, W.J.; Choi, H.S.; Kwon, H.; Kim, S.H. Recent Trends in Surface Treatment Technologies for Airframe Adhesive Bonding Processing: A Review (1995–2008). *J. Adhes.* **2010**, *86*, 192–221. [CrossRef]
14. Critchlow, G.W.; Brewis, D.M.; Emmony, D.C.; Cottam, C.A. Initial investigation into the effectiveness of CO_2-laser treatment of aluminium for adhesive bonding. *Int. J. Adhes. Adhes.* **1995**, *15*, 233–236. [CrossRef]
15. Wong, R.C.P.; Hoult, A.P.; Kim, J.K.; Yu, T.X. Improvement of adhesive bonding in aluminium alloys using a laser surface texturing process. *J. Mater. Process. Technol.* **1997**, *63*, 579–584. [CrossRef]
16. Harris, A.; Beevers, A. The effects of grit-blasting on surface properties for adhesion. *Int. J. Adhes. Adhes.* **1999**, *19*, 445–452. [CrossRef]
17. Lefebvre, D.; Ahn, B.; Dillard, D.; Dillard, J. The effect of surface treatments on interfacial fatigue crack initiation in aluminum/epoxy bonds. *Int. J. Fract.* **2002**, *114*, 191–202. [CrossRef]
18. Park, S.Y.; Choi, W.J.; Choi, H.S.; Kwon, H. Effects of surface pre-treatment and void content on GLARE laminate process characteristics. *J. Mater. Process. Technol.* **2010**, *210*, 1008–1016. [CrossRef]

19. Ning, H.; Li, Y.; Hu, N.; Cao, Y.; Yan, C.; Azuma, T.; Peng, X.; Wu, L.; Li, J.; Li, L. Improvement of the mode II interface fracture toughness of glass fiber reinforced plastics/aluminum laminates through vapor grown carbon fiber interleaves. *Sci. Technol. Adv. Mater.* **2014**, *15*, 035004. [CrossRef]
20. Khan, S.U.; Kim, J.-K. Improved interlaminar shear properties of multiscale carbon fiber composites with bucky paper interleaves made from carbon nanofibers. *Carbon* **2012**, *50*, 5265–5277. [CrossRef]
21. Kinloch, A.; Little, M.; Watts, J. The role of the interphase in the environmental failure of adhesive joints. *Acta Mater.* **2000**, *48*, 4543–4553. [CrossRef]
22. Ning, H.; Iijima, T.; Hu, N.; Liu, Y.; Wu, L.; Liu, F.; Arai, M. Investigation on mode-II interface fracture toughness of CFRP/Al laminates toughened by VGCF interleaves. *J. Mater. Sci.* **2015**, *50*, 1915–1923. [CrossRef]
23. Ning, H.; Li, Y. Improvement of interlaminar mechanical properties of CARALL based on nanofiller interface reinforcement and other fabrication techniques. In Proceedings of the ICF13, Beijing, China, 16–21 June 2013.
24. Sun, Z.; Jeyaraman, J.; Sun, S.; Hu, X.; Chen, H. Carbon-fiber aluminum-foam sandwich with short aramid-fiber interfacial toughening. *Compos. Part A Appl. Sci. Manuf.* **2012**, *43*, 2059–2064. [CrossRef]
25. Shi, S.-S.; Sun, Z.; Hu, X.-Z.; Chen, H.-R. Carbon-fiber and aluminum-honeycomb sandwich composites with and without Kevlar-fiber interfacial toughening. *Compos. Part A Appl. Sci. Manuf.* **2014**, *67*, 102–110. [CrossRef]
26. Sun, Z.; Hu, X.; Chen, H. Effects of aramid-fibre toughening on interfacial fracture toughness of epoxy adhesive joint between carbon-fibre face sheet and aluminium substrate. *Int. J. Adhes. Adhes.* **2014**, *48*, 288–294. [CrossRef]
27. Sun, Z.; Shi, S.; Hu, X.; Guo, X.; Chen, J.; Chen, H. Short-aramid-fiber toughening of epoxy adhesive joint between carbon fiber composites and metal substrates with different surface morphology. *Compos. Part B Eng.* **2015**, *77*, 38–45. [CrossRef]
28. Ning, H.; Li, Y.; Hu, N.; Arai, M.; Takizawa, N.; Liu, Y.; Wu, L.; Li, J.; Mo, F. Experimental and numerical study on the improvement of interlaminar mechanical properties of Al/CFRP laminates. *J. Mater. Process. Technol.* **2015**, *216*, 79–88. [CrossRef]
29. Nguyen, A.T.; Brandt, M.; Orifici, A.C.; Feih, S. Hierarchical surface features for improved bonding and fracture toughness of metal–metal and metal–composite bonded joints. *Int. J. Adhes. Adhes.* **2016**, *66*, 81–92. [CrossRef]
30. Nguyen, A.T.; Brandt, M.; Feih, S.; Orifici, A.C. Pin pull-out behaviour for hybrid metal-composite joints with integrated reinforcements. *Compos. Struct.* **2016**, *155*, 160–172. [CrossRef]
31. Cui, Q.; Gao, F.; Mukherjee, S.; Gu, Z. Joining and interconnect formation of nanowires and carbon nanotubes for nanoelectronics and nanosystems. *Small* **2009**, *5*, 1246–1257. [CrossRef] [PubMed]
32. Peng, P.; Hu, A.; Gerlich, A.P.; Zou, G.; Liu, L.; Zhou, Y.N. Joining of silver nanomaterials at low temperatures: Processes, properties, and applications. *ACS Appl. Mater. Interfaces* **2015**, *7*, 12597–12618. [CrossRef] [PubMed]
33. Hu, A.; Guo, J.; Alarifi, H.; Patane, G.; Zhou, Y.; Compagnini, G.; Xu, C. Low temperature sintering of Ag nanoparticles for flexible electronics packaging. *Appl. Phys. Lett.* **2010**, *97*, 153117. [CrossRef]
34. Bai, J.G.; Zhang, Z.Z.; Calata, J.N.; Lu, G.-Q. Low-temperature sintered nanoscale silver as a novel semiconductor device-metallized substrate interconnect material. *IEEE Trans. Compon. Packag. Technol.* **2006**, *29*, 589–593. [CrossRef]
35. Ide, E.; Angata, S.; Hirose, A.; Kobayashi, K.F. Metal–metal bonding process using Ag metallo-organic nanoparticles. *Acta Mater.* **2005**, *53*, 2385–2393. [CrossRef]
36. Kobayashi, Y.; Abe, Y.; Maeda, T.; Yasuda, Y.; Morita, T. A metal–metal bonding process using metallic copper nanoparticles produced by reduction of copper oxide nanoparticles. *J. Mater. Res. Technol.* **2014**, *3*, 114–121. [CrossRef]
37. Wakuda, D.; Hatamura, M.; Suganuma, K. Novel method for room temperature sintering of Ag nanoparticle paste in air. *Chem. Phys. Lett.* **2007**, *441*, 305–308. [CrossRef]
38. Yan, J.; Zou, G.; Wu, A.-p.; Ren, J.; Yan, J.; Hu, A.; Zhou, Y. Pressureless bonding process using Ag nanoparticle paste for flexible electronics packaging. *Scr. Mater.* **2012**, *66*, 582–585. [CrossRef]
39. Peng, P.; Hu, A.; Zhao, B.; Gerlich, A.P.; Zhou, Y.N. Reinforcement of Ag nanoparticle paste with nanowires for low temperature pressureless bonding. *J. Mater. Sci.* **2012**, *47*, 6801–6811. [CrossRef]

40. NormanáZhou, Y. Room-temperature pressureless bonding with silver nanowire paste: Towards organic electronic and heat-sensitive functional devices packaging. *J. Mater. Chem.* **2012**, *22*, 12997–13001.
41. Garnett, E.C.; Cai, W.; Cha, J.J.; Mahmood, F.; Connor, S.T.; Christoforo, M.G.; Cui, Y.; McGehee, M.D.; Brongersma, M.L. Self-limited plasmonic welding of silver nanowire junctions. *Nat. Mater.* **2012**, *11*, 241. [CrossRef] [PubMed]